IEEE Access
Multidisciplinary | Rapid Review | Open Access Journal

Received June 16, 2020, accepted June 30, 2020, date of publication July 6, 2020, date of current version August 3, 2020.

Digital Object Identifier 10.1109/ACCESS.2020.3007169

Few-Mode Fibers With Uniform Differential Mode Group Delay for Microwave Photonic Signal Processing

JIAN ZHAO[1], HUAN ZHANG[1], ZHIQUN YANG[1], JINSHENG XU[1], TIANHUA XU[1,2], AND CHAO WANG[3], (Member, IEEE)

[1]Key Laboratory of Opto-Electronics Information Technology, School of Precision Instrument and Optoelectronics Engineering, Ministry of Education, Tianjin University, Tianjin 300072, China
[2]School of Engineering, University of Warwick, Coventry CV4 7AL, U.K.
[3]School of Engineering and Digital Arts, University of Kent, Canterbury CT2 7NT, U.K.

Corresponding authors: Jian Zhao (enzhaojian@tju.edu.cn) and Chao Wang (c.wang@kent.ac.uk)

This work was supported in part by the National Natural Science Foundation of China (NSFC) under Grant 61775165 and Grant 61975248, and in part by the Engineering and Physical Sciences Research Council (EPSRC) of U.K. under Grant EP/S005625/1.

ABSTRACT We present a novel design of few-mode fiber (FMF) with a uniform differential mode group delay (U-DMGD) among propagating modes and apply the FMF to a single-fiber delay line module for implementing microwave photonic finite impulse response (FIR) filters. By optimizing key parameters such as the core grading exponent and the dimension of the trench of FMF, a U-DMGD between adjacent modes among four modes (LP_{01}, LP_{11}, LP_{02} and LP_{31}) over the entire C band is achieved. Wavelength dependence is entirely removed. An FIR microwave photonic filter (MPF) implemented using the designed 1-km FMF is investigated through numerical simulations. The free spectral range (FSR) of the MPF is 5.7 GHz, the 3-dB bandwidth is 1.26 GHz, and the main lobe-to-side lobe ratio (MSR) is 10.42 dB. Discussions on fabrication aspects have also been presented. The proposed single-fiber delay line structure based on FMF can significantly reduce the system complexity of microwave photonic signal processing.

INDEX TERMS Few-mode fiber, uniform differential mode group delay (U-DMGD), delay line, microwave photonic filter (MPF).

I. INTRODUCTION

The microwave photonic filter (MPF), which is a pivotal module in microwave photonics, has been applied in various fields such as radar, phased array beamforming and radio over fiber networks etc [1]. As a dominate branch of MPFs, the tapped transverse MPF uses a set of finitely or infinitely weighted and differentially delayed optical signals to carry the same microwave signal. After photodetection, the summation of these weighted and delayed microwave signal copies leads to a required microwave filter transfer function [2]. A typical finite impulse response (FIR) MPF architecture is shown in Fig. 1. Input RF signals are modulated onto optical carrier through the intensity modulator. The modulated signals are divided into N channels, and the signals in each channel passes through attenuators and differentially delayed fibers to adjust the signal weights and delays. The N-channel optical delay lines are recombined using a standard N×1 fused fiber coupler [2]. Finally, the signals are detected by a photodetector (PD). According to the number of light sources, FIR MPFs can be divided into two categories, single-source MPFs and multi-source MPFs. For single-source MPFs, optical interference effects adversely impact the performance of MPFs, where the differential optical delay is smaller than the coherence time of the source. In order to avoid the optical interference effects, MPF source devices, such as fiber Bragg gratings and multi-wavelength sources, are implemented in the incoherent regime [3]. However, these methods will increase the complexity and cost of the fabrication.

On the other hand, the development of spatial division multiplexing (SDM) technologies including multi-core multiplexing (MCM) [4], mode division multiplexing (MDM) [5] and their successful application in optical fiber communication systems have brought new opportunities for microwave photonic subsystems such as MPFs. In the case of MCM, an MPF has been proposed based on the selective inscription of Bragg grating in homogeneous multicore fibers. The multi-core fiber includes N cores engraved with M gratings,

The associate editor coordinating the review of this manuscript and approving it for publication was Sukhdev Roy.

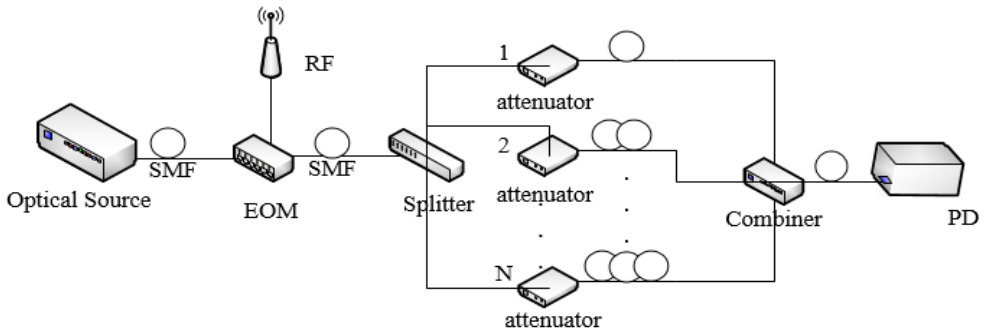

FIGURE 1. The FIR filter architecture with individually weighted and differentially delayed taps.

so this device offers a total of N×M delayed signal samples [6]. Meanwhile, an FMF based MPF was also experimentally demonstrated [7]. The MPF utilized DMGDs as optical delay lines, and the amplitudes of the modes excited by the higher-order mode (HOM) excitation method are employed as the tap weights of the filter. In addition, an MPF was realized by determining the wavelength according to the uniform DMGD between adjacent modes and the inscription of the long period grating (LPG) at a specific longitudinal position along the fiber [8], [9]. However, it is crucial to select the specific wavelength or implement LPGs to achieve U-DMGD between adjacent modes. As the number of modes increases, it is more and more difficult and complex to control the operation wavelength.

In this paper, we present a novel optimization scheme of the FMF with U-DMGD over the C band. The proposed FMF supports four modes: LP_{01}, LP_{11}, LP_{02} (LP_{21}), and LP_{31} (LP_{12}). Compared to delay line elements based on the single-mode fiber (SMF), the delay line elements based on the proposed FMF offers a higher dispersion efficiency, a better power handling capability and less nonlinear effects [7]. Correspondingly, the MPF based on the FMF with U-DMGD is theoretically analyzed, and the spectral response of the MPF is obtained. Compared to the reported designs [8], [9], the MPF can employ the mode dispersion and the chromatic dispersion to provide the uniform time delay difference for signals at different modes and wavelengths, and can thus increase its number of taps. This paper is organized as follows: Section 2 introduces the design strategy of the FMF with U-DMGD; Section 3 introduces the optimization process of the FMF with U-DMGD; Section 4 presents the schematic setup and spectral response of the MPF with U-DMGD FMF; Section 5 draws conclusions of the paper.

II. DESIGN STRATEGY OF FMF WITH U-DMGD

The definitions of the geometry and parameters in the U-DMGD FMF are described below. The U-DMGD FMF consists of four regions: core (CO), inner cladding (IC), trench (TR) and outer cladding (CL), as shown in Fig. 2. The radii of the core, the inner cladding, the trench and the cladding are represented using R_{CO}, R_{IC}, R_{TR}, and R_{CL}, respectively.

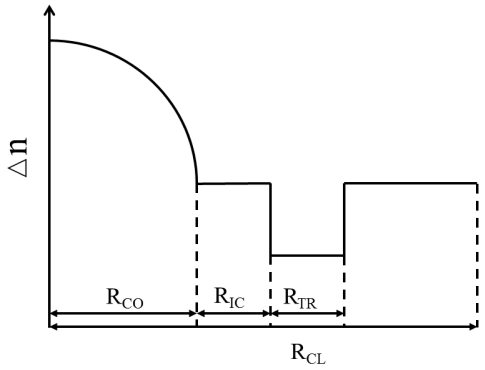

FIGURE 2. The illustrative schematic of the refractive index profile.

The refractive index profile of the U-DMGD FMF, composed by a graded-index core region and a step-index cladding trench region, is described by:

$$n(r) = \begin{cases} n_{CO}[1 - \Delta n_{CO}(\dfrac{r}{R_{CO}})^{\alpha}] \\ \quad 0 < r < R_{CO} \\ n_{CL} \\ \quad R_{CO} < r < R_{CO} < R_{IC} \\ \dfrac{n_{CL}}{1 - \Delta n_{TR}} \\ \quad R_{CO} + R_{IC} < r < R_{CO} + R_{IC} + R_{TR} \\ n_{CL} \\ \quad R_{CO} + R_{IC} + R_{TR} < r < R_{CL} \end{cases} \tag{1}$$

where $n(r)$ is the refractive index as a function of the radial distance r, n_{CL} is the cladding refractive index, α is the core grading exponent, and n_{CO} and Δn_{TR} are the relative refractive index differences at $r = 0$ and at the trench, respectively. The relative refractive index difference is defined as $n(r) = (n(r) - n_{CL})/n(r)$. The refractive index profile is shown in Fig. 2. Considering the traditional fiber manufacture technology and the influence of the trench on the propagating modes [10], fiber parameters are subject to the following constraints:

$$\begin{cases} 1.5 < \alpha < 2.5 \\ -0.0045 \le \Delta n_{TR} \le 0 \\ 0 \le R_{IC} \le \dfrac{1}{2} R_{CO} \\ 0 \le R_{TR} \le R_{CO} \end{cases} \tag{2}$$

The range of α is specified in (2) and $\alpha = 2$ is typical for FMFs. Since a deeper trench will be difficult to fabricate, (2) constrains n_{TR} to be greater than -0.0045. In (2), R_{IC} is limited to be $R_{CO}/2$ as a trench further away from the core has much reduced impact on the guided modes. A wider trench will make the fabrication more challenging, so R_{TR} is generally chosen to be smaller than R_{CO}. The wavelength range is bounded according to the C-band wavelengths of from 1530 nm to 1565 nm.

The normalized cutoff frequency V determines the number of modes in a graded index fiber, and can be described by [11]:

$$V = \frac{\frac{2\pi R_{CO}}{\lambda}\sqrt{n_{CO}^2 - n_{CL}^2}}{\sqrt{1+\frac{2}{\alpha}}} \tag{3}$$

In order to support four modes (LP_{01}, LP_{11}, LP_{02} and LP_{31}), the normalized cutoff frequency range is $5.8 \leq V \leq 7.2$. R_{CO} should be as large as possible to reduce the nonlinear coefficients for all modes. A core radius of FMF, $R_{CO} = 19.6\ \mu$m, is applied. The material of the cladding is set to be SiO_2. The center of the CO is GeO_2-doped SiO_2 corresponding to a 4.5% molecular fraction of GeO_2 in SiO_2. The fiber diameter is designed to be 125 μm, which refers to a typical diameter of the standard single mode fiber.

According to the definition of group delay between adjacent modes,

$$DMGD = \frac{L}{v_{g1}} - \frac{L}{v_{g2}} = \frac{L}{\frac{c}{n_{g1}}} - \frac{L}{\frac{c}{n_{g2}}} = \frac{L}{c}(n_{g1} - n_{g2}) \tag{4}$$

where L is the transmission distance, υ_{g1} and υ_{g2} are the group velocities of two modes, respectively, n_{g1} and n_{g2} are the group refractive indices of corresponding modes, respectively, and c is the speed of light in vacuum.

From (4) we have,

$$\Delta v_g = \frac{v_{g2}v_{g1}}{c}\Delta n_g \tag{5}$$

where $\upsilon_g = \upsilon_{g2} - \upsilon_{g1}$ and $n_g = n_{g1} - n_{g2}$. Since g_1 and g_2 are very close and both are much larger than υ_g, the product $\upsilon_{g2} \times \upsilon_{g1}$ can be almost considered as a constant. Therefore, the group velocity difference Δu_g is proportional to the group refractive index difference Δn_g. To achieve a U-DMGD among adjacent modes, it is necessary to achieve a uniform differential group refractive index Δn_g among adjacent modes.

Simulations of the designed fiber structure are carried out using COMSOL Multiphysics based on the full vector finite element analysis. COMSOL Multiphysics is a general-purpose simulation software for modeling designs, devices, and processes in all fields of engineering, manufacturing, and scientific research. Within the structural parameters, it is found that that the differential effective refractive index between the adjacent modes in different mode groups, such as LP_{01}-LP_{11}, LP_{02}-LP_{11} and LP_{31}-LP_{02}, is $\sim 10^{-3}$, while the effective refractive index difference between the adjacent modes in the same mode group, such as LP_{21}-LP_{02} and LP_{12}-LP_{31}, is $\sim 10^{-5}$. Subsequent investigations are all performed based on the modes of the different mode groups, unless specified.

III. PARAMETERS OPTIMIZATION OF FMF WITH U-DMGD

In order to investigate the optimum value of the core grading exponent α and the dimensions of the trench (R_{IC}, R_{TR}, and n_{TR}) that allows U-DMGD among the modes, an optimization function J is introduced with an objective of minimizing Δn_g at a specific wavelength:

$$J(R_{IC}, \alpha, \Delta n_{TR}, R_{TR}) = (\Delta n_g^{LP02-LP11} - \Delta n_g^{LP11-LP01})^2 + (\Delta n_g^{LP31-LP02} - \Delta n_g^{LP11-LP01})^2 \tag{6}$$

We firstly analyzed the impact of the R_{IC}, α, R_{TR}, and Δn_{TR} on Δn_g. A change in the structural parameter α will result in a change in the refractive index profile of the core, thereby will affect n_g of all modes. As the LP_{01} mode is mainly confined in the core, the other three structural parameters (R_{IC}, R_{TR}, and Δn_{TR}) have much less influence on the LP_{01} mode, and will mainly affect high-order modes.

Based on the explanation presented above, we studied the effect of four parameters (R_{IC}, α, R_{TR}, and n_{TR}) on J at a selected wavelength of 1550 nm, in order to realize the design of the FMF with U-DMGD.

In particular, we first fix the parameters with $\alpha = 2.1$, $R_{TR} = 3\ \mu$m, $\Delta n_{TR} = -1.5 \times 10^{-3}$ and sweep the parameter R_{IC} (from 1 μm to 3.2 μm with a step of 0.2 μm). The impact of R_{IC} on J at the wavelength of 1550 nm is shown in Fig. 3(a), where the value of J increases as R_{IC} increases. The difference of Δn_g between adjacent modes becomes greater as the distance from the core to trench increases, because the influence of the trench on each mode becomes smaller and smaller. We then fix the parameters with $R_{TR} = 3\ \mu$m, $R_{IC} = 1\ \mu$m, $\Delta n_{TR} = -1.5 \times 10^{-3}$. The effect of α (from 2.0 to 2.4 with a spacing of 0.1) on J is shown in Fig. 3(b). It can be clearly seen that when α increases, the value of J first drops and then rises. The curve shows that the value of J has a minimum value near $\alpha = 2.1$ for $\Delta n_{TR} = -1.5 \times 10^{-3}$, $R_{TR} = 3\ \mu$m and $R_{IC} = 1\ \mu$m. Fig. 3(c) shows J as a function of R_{TR} (from 1 μm to 10 μm with a step of 1 μm), at the wavelength of 1550 nm. The value of J first decreases dramatically and then increases slowly with the increase of R_{TR} in the scenario of $R_{IC} = 1\ \mu$m, $\alpha = 2.1$, $\Delta n_{TR} = -1.5 \times 10^{-3}$. Therefore, it is concluded that when R_{TR} is around 3 μm, the value of J reaches its minimum. From Fig. 3(c), we can draw the conclusion that R_{TR} has marginal influence on the difference of Δn_g, when R_{TR} exceeds a certain value (around 3 μm). Fig. 3(d) describes the relationship between J and Δn_{TR}, in order to explain the relationship between Δn_g and Δn_{TR}. We analyzed Δn_{TR} (from -0.0045 to 0 with a step of 0.0005) and it is found that as Δn_{TR} increases, the J value decreases first and then increases at the case of $R_{IC} = 1\ \mu$m, $\alpha = 2.1$,

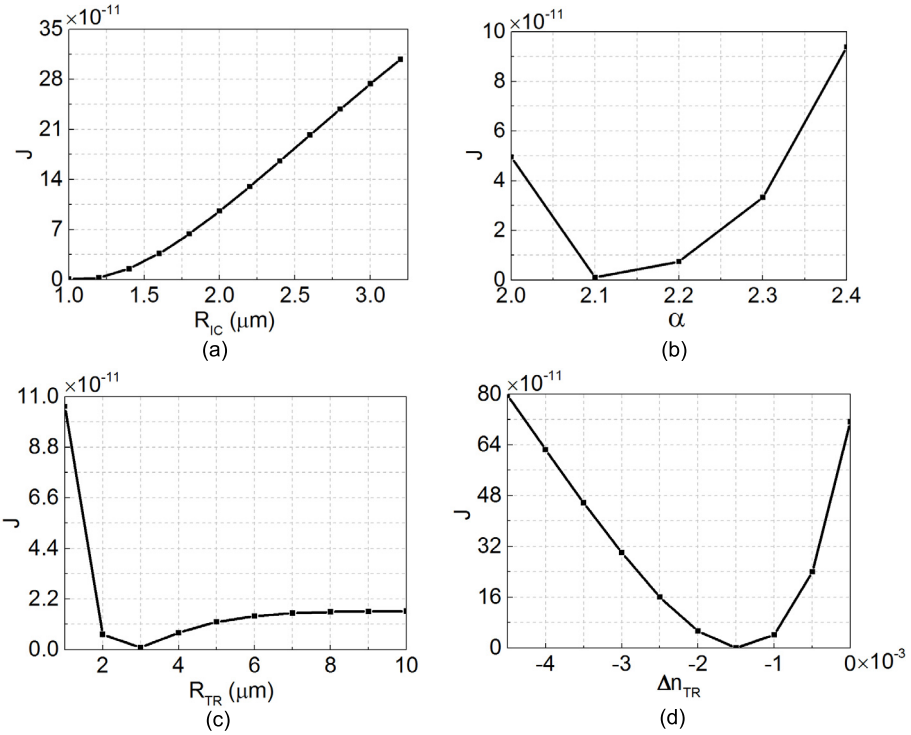

FIGURE 3. The optimization function J as a function of: (a) R_{IC}, (b) α, (c) R_{TR}, and (d) Δn_{TR} at a wavelength of 1550 nm.

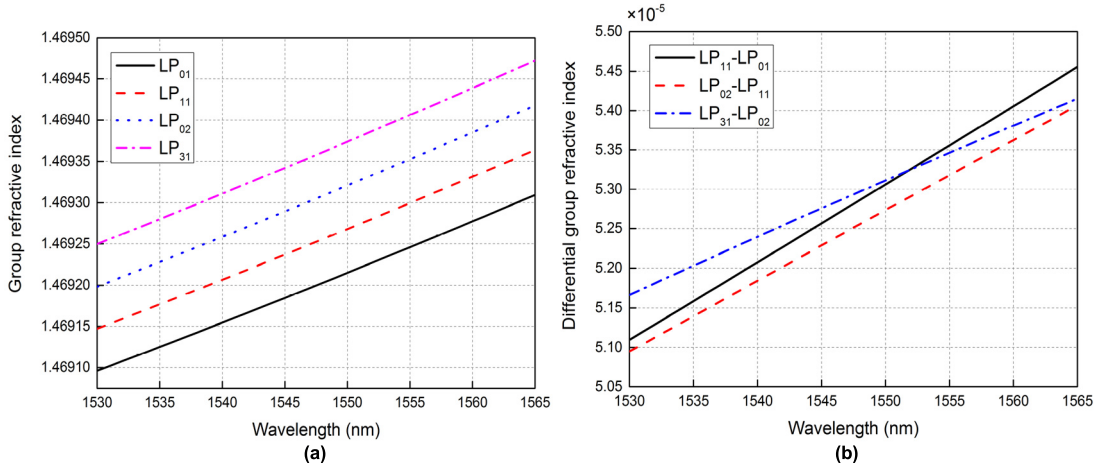

FIGURE 4. (a) n_g as a function of wavelength (b) Δn_g as a function of wavelength ranging from 1530 to 1565 nm of the optimized parameters.

$R_{TR} = 3\ \mu$m. The optimal parameter Δn_{TR} to minimizes J should be around -0.0015.

Therefore, the value of J can be minimized with adequate information of trench dimensions (R_{IC}, R_{TR}, and Δn_{TR}) and at a given wavelength. The structural parameters of the proposed FMF with U-DMGD between adjacent modes at 1550 nm are listed in Table1.

Fig. 4(a) presents n_g as a function of the wavelength based on the optimized parameters listed in Table 1(n_{CO}, n_{CL} and Δn_{TR} follow the Sellmeier Equation [12]). As shown in Fig. 4(a), Δn_g of LP_{01}, LP_{11}, LP_{02} and LP_{31} modes scale linearly with the wavelength ranging from 1530 nm to 1565 nm. We further analyze Δn_g between adjacent modes. In Fig. 4(b), $\Delta n_g^{LP11-LP01}$, $\Delta n_g^{LP02-LP11}$ and $\Delta n_g^{LP31-LP02}$

TABLE 1. The optimized parameters of an FMF to achieve uniform group-delay difference.

R_{CO}	19.6 μm
R_{IC}	1 μm
R_{TR}	3 μm
R_{CL}	62.5 μm
n_{CO}	1.4509 (1550 nm)
n_{CL}	1.444 (1550 nm)
Δn_{TR}	-1.37×10^{-3} (1550 nm)
α	2.1

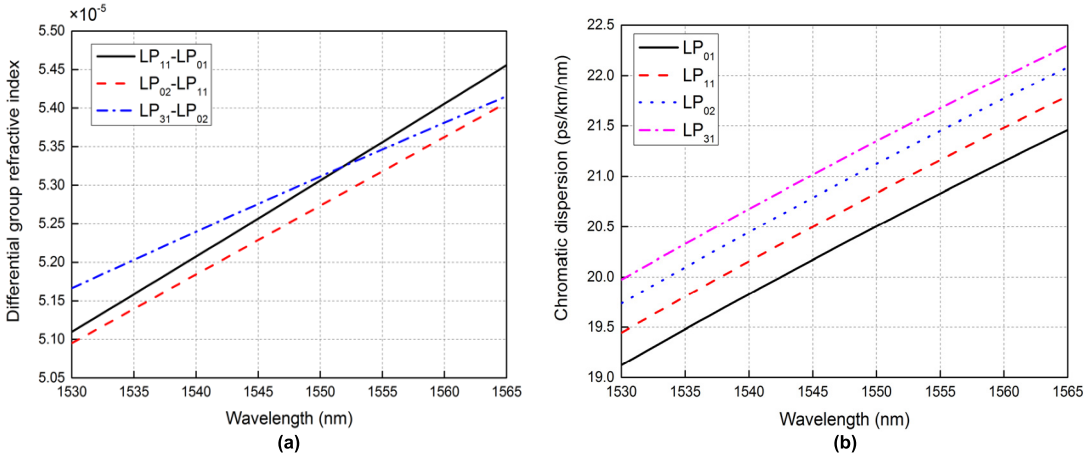

FIGURE 5. (a) DMGD (b)chromatic dispersion as a function of wavelength over the C band for the optimized parameters.

TABLE 2. Δn_{eff} and DMGD between adjacent modes at 1550 nm.

	LP_{11}-LP_{01}	LP_{02}-LP_{11}	LP_{31}-LP_{02}
Δn_{eff} ($\times 10^{-3}$)	1.18	1.21	1.19
DMGD (ps/m)	0.1769	0.1745	0.1751

increase with the increase of the wavelength, but the curves of $\Delta n_g^{LP11-LP01}$ and $\Delta n_g^{LP31-LP02}$ intersect near the wavelength of 1550 nm.

We further analyze the DMGDs per unit length between LP11 and LP01, LP02 and LP11, LP31 and LP02, which are expressed as $DMGD^{LP11-LP01}$, $DMGD^{LP02-LP11}$ and $DMGD^{LP31-LP02}$, respectively. Simulation results are shown in Fig. 5(a). The $DMGD^{LP11-LP01}$, $DMGD^{LP02-LP11}$ and $DMGD^{LP31-LP02}$ are 0.1769 ps/m, 0.1745 ps/m, 0.1751 ps/m at 1550 nm, respectively. The chromatic dispersion values of all guided modes over the C band are shown in Fig. 5(b). The Δn_{eff} and the DMGD between adjacent modes at 1550 nm are shown in Table 2.

The mode coupling effect has to be considered when a fiber is designed to provide a significant and exact delay. Δn_{eff} and DMGD between LP_{02} and LP_{21} are 1.33×10^{-5} ps/m, and 0.0048 ps/m, respectively. The overlap between the LP_{02} and the LP_{21} modes is 49.34%. The value of Δn_{eff} and DMGD between LP_{12} and LP_{31} are 1.63×10^{-5}, 0.0085 ps/m, respectively. The overlap between the LP_{12} and the LP_{31} modes is 39.66%. The mode coupling is related to the overlap integral and the effective refractive index difference [13]. The effect of the mode coupling on the proposed MPF is discussed in Section 4.

The optimized parameters in Table 1 neglect the limited precision margin of the manufacturing control process [14].

Those margins could lead to the deviation of fiber parameters from the optimized values. The typical fabrication tolerances for n_{CO}, Δn_{TR}, R_{CO}, R_{IC}, R_{TR} and α are listed in Table 3 according to [14]. These discrepancies result in corresponding deviations in the DMGD relative to the targeted value. When the deviation of each fiber parameter reaches its maximum, the DMGD of the FMF at 1550nm

TABLE 3. Typical fabrication tolerances of FMF.

R_{CO}	19.6 ± 0.49 μm
R_{IC}	1 ± 0.025 μm
R_{TR}	3 ± 0.075 μm
R_{CL}	62.5 μm
n_{CO}	1.4509 ± 0.0001 (1550 nm)
n_{TR}	$-1.37\times10^{-3} \pm 0.0001$
α	2.1 ± 0.01

is analyzed. The deviation of DMGD reach the largest value when $R_{CO} = 20.09$ μm, n_{CO} =1.4508, α = 2.09, R_{IC} = 0.075 μm, R_{TR} = 3.075 μm, Δn_{TR} = -1.38×10^{-3} at 1550 nm. The $DMGD^{LP11-LP01}$, $DMGD^{LP02-LP11}$ and $DMGD^{LP31-LP02}$ are 0.179 ps/m, 0.182 ps/m, 0.185 ps/m, respectively. The difference of DMGD is 0.003 ps/m.

IV. SETUP OF MPF AND PERFORMANCE EVALUATION

Since we lack of the fiber manufacturing facility, numerical simulations using VPItransmissionMaker software have been implemented to verify the utitlity of the designed FMF in MPF systems. Realistic fibre parameters have been selected in the simulation and the stated manufacturing tolerances have been considered. Studies in the previous papers have shown that when the bending radius of the FMF is not particularly small, light propagation loss and mode crosstalk can be ignored [15], [16]. The system setup is shown in Fig. 6. The MPF is composed of an RF signal source, a laser, a Mach-Zehnder modulator, a mode multiplexer, a photodetector, a vector network analyzer and 1-km FMF with U-DMGD.

The characteristic parameters of the FMF with U-DMGD are employed into the model. The RF signals are modulated onto the optical carriers through the intensity modulator. All modes are equally excited by the mode multiplexer and are coupled into the FMF with U-DMGD. At the receiver end, the optical signals of all modes are detected by a PD.

The normalized radio-frequency response of the MPF is obtained by the vector network analyzer as shown in Fig 7.

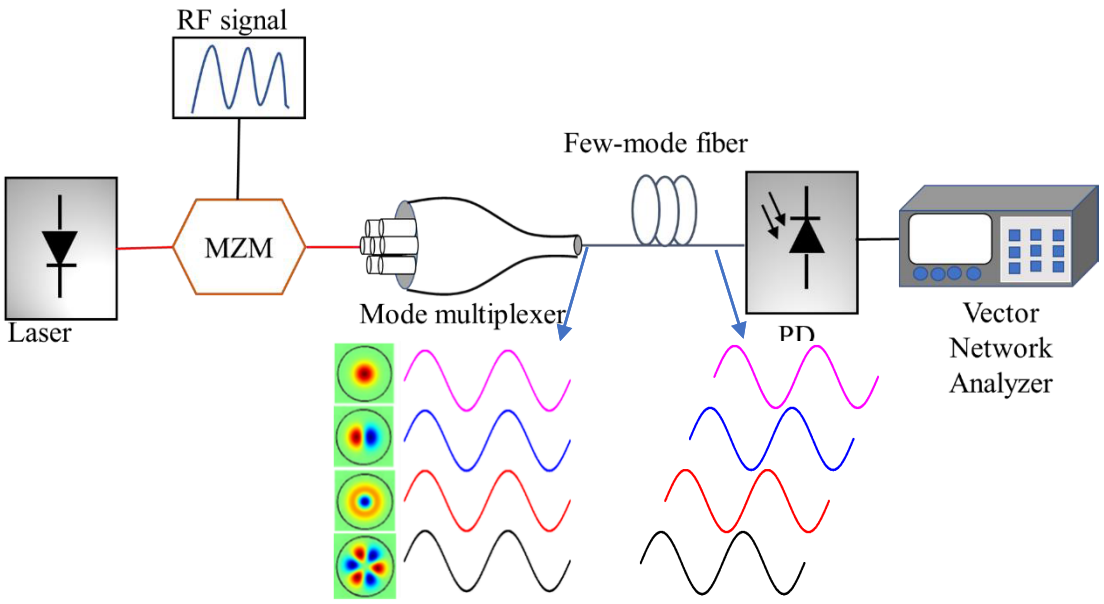

FIGURE 6. Setup of the MPF based on the FMF. RF signal: radio-frequency signal; MZM: Mach-Zehnder modulator, PD: photodetector.

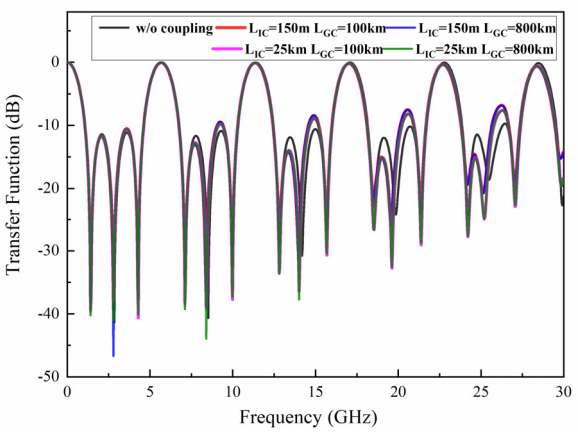

FIGURE 7. Normalized radio-frequency response of the implemented MPF. Black solid line: without coupling; red solid line: L_{IC} = 150 m, L_{GC} = 100 km; blue solid line: L_{IC} = 150 m, L_{GC} = 800 km; pink solid line: L_{IC} = 25 km, L_{GC} = 100 km; green solid line: L_{IC} = 25 km, L_{GC} = 800 km.

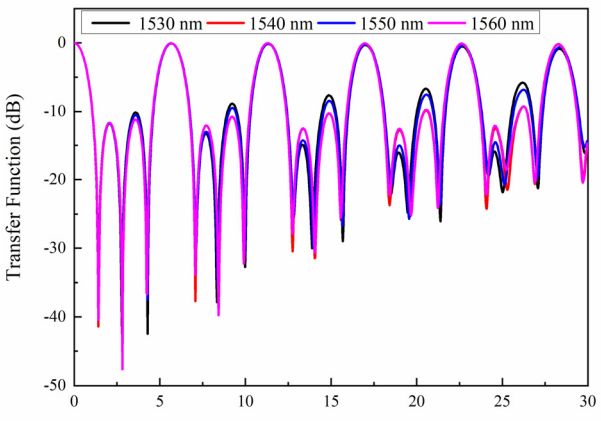

FIGURE 8. Normalized radio-frequency response of the MPF implemented at 1530 nm, 1540 nm, 1550 nm, and 1560 nm.

In Fig. 7, the black curve corresponds to the spectral response of the MPF without considering any mode coupling. However, due to the perturbation of the refractive index, the mode coupling along the FMF has to be considered. As mentioned in Section 2, the differential effective refractive index among the mode groups is in the order of 10^{-3}, which can be regarded as a case of weak coupling, while the differential effective refractive index within each mode group is in the order of 10^{-5}, which can be considered as a case of strong coupling [17]. The correlation coupling length is larger than the total system length in the weak coupling regime, while the correlation coupling length is much smaller than the total system length in the strong coupling regime [18]. We studied the impacts of the strong coupling and the weak coupling on the transfer function of the MPF. For comparison, the correlation coupling lengths within the mode group (L_{IC}) are selected as 150 m and 25 km, respectively [19]. The correlation coupling lengths between mode groups (L_{GC}) are selected as 100 km and 800 km, respectively [20], [21]. As shown in Fig. 7, the FSR of the MPF is 5.7 GHz, the 3-dB bandwidth is 1.26 GHz, and the MSR is 10.42 dB. By comparing the five curves, it is found that the FSR and the 3-dB bandwidth of the MPF remain unchanged, while the MSR of the MPF decreases due to the mode coupling.

The normalized radio-frequency response of the MPF over the C band is also analyzed. The normalized radio-frequency response functions of the MPF at 1530 nm, 1540 nm, 1550 nm, and 1560 nm are shown in Fig. 8, respectively. The L_{GC} is selected as 100 km and the L_{IC} is selected as 150 m. As shown in Fig. 8, the transfer function walks off slightly because the DMGD and the dispersion of the FMF differ slightly at different wavelengths.

In fact, the finite precision margins of the manufacturing processes cannot be neglected. Hence, the transfer function will vary with the manufacturing error [14]. The transfer

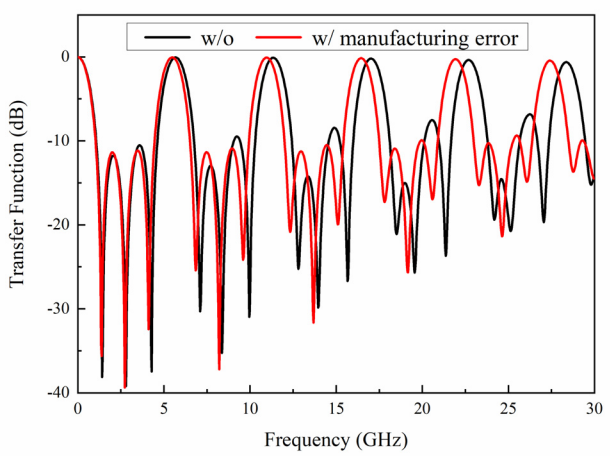

FIGURE 9. The normalized radio-frequency response of the MPF implemented. Black solid line: $R_{CO} = 19.6\ \mu$m, $n_{CO} = 1.4509$, $\alpha = 2.1$, $R_{IC} = 1\ \mu$m, $R_{TR} = 3\ \mu$m, $\Delta n_{TR} = -1.37 \times 10^{-3}$; red solid line: $R_{CO} = 20.09\ \mu$m, $n_{CO} = 1.4508$, $\alpha = 2.09$, $R_{IC} = 0.075\ \mu$m, $R_{TR} = 3.075\ \mu$m, $\Delta n_{TR} = -1.38 \times 10^{-3}$.

functions of the MPF without any manufacturing error and with a maximum manufacturing error have been simulated in Fig. 9. The parameters used are listed in Table 3. Due to the influence of the process tolerance, the DMGDs between modes will change, and the FSR and MSR of the MPF will decrease. The FSR of the MPF is reduced by 0.03 GHz.

V. CONCLUSIONS

In this paper, an FMF with U-DMGD among propagated modes is designed. Through the optimization of structural parameters, the stable excitation and transmission of four modes (LP_{01}, LP_{11}, LP_{02} and LP_{31}) with U-DMGD among them are achieved over the entire C band. The designed FMF features wavelength independent U-DMGD. As a single-fiber multitap delay line structure, the FMF holds great potential in effectively reducing the complexity of the MPF system in microwave photonic signal processing. Specifically, the deviation of fiber geometric dimensions and the doping concentrations are tolerable and reasonable within the existing fiber manufacture facility restrictions. Thus, our design is highly promising for practical fabrications. The FIR MPFs based on the U-DMGD FMF can employ the mode coupler (such as the photonic lantern) to independently adjust and control the power of each excited mode, and can thus realize the tunability of the filter response. Although the MPF based on the FMF with U-DMGD can only realize a low-pass filter response, equivalent negative or complex tap coefficients can be obtained by deliberately designing non-uniform time delays among filter taps using our proposed method, in order to realize a reconfigurable frequency response.

ACKNOWLEDGMENT

(Jian Zhao and Huan Zhang contributed equally to this work.)

REFERENCES

[1] V. Urick, K. Williams, and J. Mckinney, *Fundamentals of Microwave Photonics*. Hoboken, NJ, USA: Wiley, 2015.
[2] J. Capmany, J. Mora, I. Gasulla, J. Sancho, J. Lloret, and S. Sales, "Microwave photonic signal processing," *J. Lightw. Technol.*, vol. 31, no. 4, pp. 571–586, Feb. 15, 2013.
[3] J. Yao, "Photonics to the rescue: A fresh look at microwave photonic filters," *IEEE Microw. Mag.*, vol. 16, no. 8, pp. 46–60, Sep. 2015.
[4] J. Sakaguchi, B. J. Puttnam, W. Klaus, Y. Awaji, N. Wada, A. Kanno, and T. Kawanishi, "Large-scale space division multiplexed transmission through multi-core fiber," in *Proc. Asia Commun. Photon. Conf.*, 2012, pp. 1–3, Paper AS2C.5.
[5] S. Berdagué and P. Facq, "Mode division multiplexing in optical fibers," *Appl. Opt.*, vol. 21, no. 11, pp. 1950–1955, 1982.
[6] I. Gasulla, D. Barrera, J. Hervás, and S. Sales, "Spatial division multiplexed microwave signal processing by selective grating inscription in homogeneous multicore fibers," *Sci. Rep.*, vol. 7, no. 1, Mar. 2017, Art. no. 41727.
[7] D. V. Nickel, C. Villarruel, K. Koo, F. Bucholtz, and B. Haas, "Few mode fiber-based microwave photonic finite impulse response filters," *J. Lightw. Technol.*, vol. 35, no. 23, pp. 5230–5236, Dec. 1, 2017.
[8] S. Garcia, R. Guillem, R. Madrigal, J. Barrera, D. Barrera, S. Sales, and I. Gasulla, "Sampled true time delay line operation by inscription of long period gratings in few-mode fibers," *Opt. Express*, vol. 27, no. 16, pp. 22787–22793, 2018.
[9] R. Guillem, S. Garcia, R. Madrigal, J. Barrera, D. Barrera, and I. Gasulla, "Few-mode fiber true time delay lines for distributed radiofrequency signal processing," *Opt. Express*, vol. 26, no. 20, pp. 25761–25768, 2019.
[10] F. M. Ferreira, D. Fonseca, and H. J. A. da Silva, "Design of few-mode fibers with M-modes and low differential mode delay," *J. Lightw. Technol.*, vol. 32, no. 3, pp. 353–360, Feb. 1, 2014.
[11] V. A. Bhagavatula, "Estimation of single-mode waveguide dispersion using an equivalent-step-index approach," *Electron. Lett.*, vol. 18, no. 8, pp. 319–320, Apr. 1982.
[12] V. Brückner, *To the Use of Sellmeier Formula*, vol. 42. Bonn, Germany: Senior Experten Service (SES), 2011, pp. 242–250.
[13] G. Li, N. Bai, N. Zhao, and C. Xia, "Space-division multiplexing: The next frontier in optical communication," *Adv. Opt. Photon.*, vol. 6, no. 4, pp. 413–487, 2014.
[14] F. Ferreira, D. Fonseca, and H. Silva, "Design of few-mode fibers with arbitrary and flattened differential mode delay," *IEEE Photon. Technol. Lett.*, vol. 25, no. 5, pp. 438–441, Mar. 1, 2013.
[15] J. Han, G. Gao, Y. Zhao, and S. Hou, "Bend performance analysis of few-mode fibers with high modal multiplicity factors," *J. Lightw. Technol.*, vol. 35, no. 13, pp. 2526–2534, Jul. 1, 2017.
[16] J. A. Jay, "An overview of macrobending and microbending of optical fibers," Corning, Corning, NY, USA, White Paper, 2010, pp. 1–21.
[17] J. Zhao, I. Kim, O. Vassilieva, T. Ikeuchi, W. Wang, H. Wen, and G. Li, "Minimizing the number of spans for terrestrial fiber-optic systems using quasi-single-mode transmission," *IEEE Photon. J.*, vol. 10, no. 1, pp. 1–10, Feb. 2018.
[18] K.-P. Ho and J. M. Kahn, "Linear propagation effects in mode-division multiplexing systems," *J. Lightw. Technol.*, vol. 32, no. 4, pp. 614–628, Feb. 15, 2014.
[19] S. Kawakami and H. Tanji, "Evolution of power distribution in graded-index fibres," *Electron. Lett.*, vol. 19, no. 3, pp. 100–102, Feb. 1983.
[20] F. Ferreira, S. Sygletos, and A. Ellis, "Impact of linear mode coupling on the group delay spread in few-mode fibers," in *Proc. Opt. Fiber Commun. Conf.*, 2015, pp. 1–3, Paper Tu2D.1.
[21] T. Mori, T. Sakamoto, M. Wada, T. Yamamoto, and F. Yamamoto, "Low DMD four LP mode transmission fiber for wide-band WDM-MIMO system," in *Proc. Opt. Fiber Commun. Conf.*, 2015, pp. 1–3, Paper OTh3K.1.

JIAN ZHAO received the M.S. degree from Nankai University, in 2006, and the Ph.D. degree from The Hong Kong Polytechnic University, in 2010. He is currently an Associate Professor with the School of Precision Instruments and Optoelectronics Engineering, Tianjin University. He has authored or coauthored more than 50 articles in peer-reviewed journals and leading international conferences. His current research interests include optical fiber communications, optical fiber sensing, and nonlinear optics.

HUAN ZHANG received the B.S. degree from Hebei University, in 2017. She is currently pursuing the M.S. degree with Tianjin University. Her current research interests include optical fiber communications, optical fiber sensing, and nonlinear optics.

ZHIQUN YANG received the B.S. degree from the Dalian University of Technology and the M.S. and Ph.D. degrees from Tianjin University, in 2019. Since 2019, he has been working with Tianjin University. His research interests include fiber communication, signal processing, and RF photonics.

JINSHENG XU received the B.S. degree from the School of Precision Instruments and Optoelectronics Engineering, Tianjin University, in 2019, where he is currently pursuing the master's degree with the School of Computer Science and Engineering. His research interests include optical fiber communications, optical fiber sensing, and nonlinear optics.

TIANHUA XU received the B.Eng. degree in information engineering and the M.Sc. degree in optical engineering from Tianjin University, in 2005 and 2008, respectively, and the Ph.D. degree from the School of Information and Communication Technology, Royal Institute of Technology (KTH), in 2012. He has published over 90 journal articles and conference papers, and two book chapters. He holds four patents. His current research interests include optical communication networks, digital signal processing, machine learning, information theory, and nonlinear fiber optics. He has been the TPC Co-Chair/member of over 20 IEEE conferences and a member of the IEEE ComSoc and IPS, the International Society for Optical Engineering, and the Optical Society of America.

CHAO WANG (Member, IEEE) received the B.Eng. degree in optoelectrical engineering from Tianjin University, Tianjin, China, in 2002, the M.Sc. degree in optics from Nankai University, Tianjin, in 2005, and the Ph.D. degree in electrical and computer engineering from the University of Ottawa, Canada, in 2011. From 2011 to 2012, he was an NSERC Postdoctoral Fellow of the Photonics Laboratory, University of California at Los Angeles, Los Angeles, CA, USA. He was appointed as a Lecturer with the School of Engineering and Digital Arts, University of Kent, Canterbury, U.K., where he became a Senior Lecturer, in 2017. He has authored more than 100 articles in peer-reviewed journals and leading international conferences. His research interests include microwave photonics, ultrafast imaging, optical communications, optical sensing, and biophotonics for scientific and engineering applications. He is a Chartered Engineer (C.Eng.) of the IET and a Fellow of the Higher Education Academy (HEA), U.K. He also served as a TPC Member of MWP conferences, in 2017 and 2019. He was the recipient of the IEEE Photonics Society Graduate Student Fellowship, in 2009, the Vanier Canada Graduate Scholarship, in 2009, the Natural Sciences and Engineering Research Council (NSERC) of Canada Postdoctoral Fellowship, in 2010, the IEEE MTT-S Graduate Fellowship, in 2010, and the EU Marie-Curie Career Integration Grant, in 2014. He is a Technical Program Committee (TPC) Co-Chair of the Optoelectronics Global Conference (OGC), in 2019. He was a Guest Editor of a special section on Microwave Photonics in Optical Engineering, in 2015, and a Lead Guest Editor of a special issue on Microwave Photonics in MDPI Photonics, in 2017. He is an Associate Editor of the IEEE PHOTONICS TECHNOLOGY LETTERS.